AGU PUBLICATIONS

Geophysical Research Letters

RESEARCH LETTER
10.1002/2016GL068893

Key Points:
- Fluid pressurization is less effective at inducing accelerated slip events than mechanical reduction in normal stress
- Fluid pressurization enhances slip events by increasing the rate at which effective normal stress decreases
- During slip events, slip rate and shear stress drop are correlated with fluid pressurization rate and not the magnitude of fluid pressure

Supporting Information:
- Supporting Information S1

Correspondence to:
M. E. French,
mefrench@umd.edu

Citation:
French, M. E., W. Zhu, and J. Banker (2016), Fault slip controlled by stress path and fluid pressurization rate, *Geophys. Res. Lett.*, *43*, 4330–4339, doi:10.1002/2016GL068893.

Received 29 NOV 2015
Accepted 20 APR 2016
Accepted article online 25 APR 2016
Published online 7 MAY 2016

Fault slip controlled by stress path and fluid pressurization rate

Melodie E. French[1], Wenlu Zhu[1], and Jeremy Banker[1]

[1]Department of Geology, University of Maryland, College Park, Maryland, USA

Abstract The practice of injecting fluids into the crust is linked to regional increases in seismicity. Increasing fluid pressure along preexisting faults is believed to enhance seismicity rates by reducing the shear stress required for slip, but the processes that cause faults to slip under conditions of fluid pressurization are poorly constrained. We use experimental rock deformation to investigate the controls of fluid pressurization and pressurization rates on fault slip style. We show that pore fluid pressurization is less effective that mechanical changes in fault normal stress at initiating accelerated slip events. Fluid pressurization enhances the total slip, slip velocity, and shear stress drop of events initiated by mechanical changes in normal stress, and these parameters are correlated with pressurization rate, but not the magnitude of fluid pressure. This result is consistent with field-scale observations and indicates that processes active at the pore network scale affect induced seismicity.

1. Introduction

Fault reactivation occurs when pore fluid pressure increases as a result of natural fluid sources [*Hubbert and Rubey*, 1959] and geologic engineering practices that include wastewater disposal [*Keranen et al.*, 2013; *Kim*, 2013], geothermal stimulation [*Majer et al.*, 2007; *Deichmann and Giardini*, 2009], and hydraulic fracturing [*Holland*, 2013]. The most common model for faulting is a threshold criterion whereby slip occurs when the shear stress along the fault, τ, reaches a critical value, τ_C. For a given fault normal stress, σ_n, the critical shear stress is $\tau_C = \mu(\sigma_n - P_f)$, where μ is the coefficient of sliding friction ($0.6 \leq \mu \leq 0.85$ for most rocks) [*Byerlee*, 1978], P_f is pore fluid pressure, and $\sigma_n' = \sigma_n - P_f$ is the "effective normal stress." Increasing pore fluid pressure by fluid injection causes a corresponding decrease in the effective normal stress and critical shear stress, and according to the threshold model, slip occurs when the critical shear stress is reduced to the resolved shear stress along the fault.

Although it is clear that regional increases in seismicity rates are correlated with increased fluid injection activities [*Keranen et al.*, 2013; *Kim*, 2013; *Brodsky and Lajoie*, 2013; *Petersen et al.*, 2015], in most cases fluid injection does not cause earthquakes that can be felt at the surface either because fault slip does not occur or slip is aseismic [*Ellsworth*, 2013]. Thus, efforts to minimize the effects of induced seismicity focus on understanding the fundamental processes and geologic factors that cause faults to slip seismically during fluid injection. Geophysical observations show regional differences in the efficiency with which fluid injection induces seismicity [*Frohlich et al.*, 2015], indicating that local and regional geology such as the presence of faults preferably oriented for slip are important controls [*Horton*, 2012; *Kim*, 2013]. The moment magnitude and magnitude distribution of seismic slip events have been correlated with the rate of fluid injection and total volume of fluid injected to understand the fundamental processes by which fluids induce seismicity [*McGarr*, 1976; *Brodsky and Lajoie*, 2013; *McGarr*, 2014; *Martinez-Garzon et al.*, 2014; *Frohlich et al.*, 2015; *Weingarten et al.*, 2015]. Constraining the conditions and mechanisms that control the occurrence and style of fault slip from geophysical observation is difficult, however, because of regional differences in injection history, lithology, structure, and stress state.

The threshold model is not sufficient for modeling and predicting whether slip along a favorably oriented fault induced by fluid injection will be seismic or aseismic. We use experimental methods to investigate the fundamental processes and efficiency of increasing pore fluid pressure on inducing fault slip. We induce slip under constant and decreasing effective normal stress, to investigate the effective stress path associated with fluid injection. We compare the results of decreasing effective normal stress by reducing the mechanical load (σ_n) to increasing the pore fluid pressure (P_f) to isolate the role of evolving fluid pressure on fault slip style.

Table 1. Table of Experiments[a]

ID	Sandstone	Experiment Type	v (m/s)	σ_3 (MPa)	$d\sigma_3/dt$ (MPa/min)	P_f (MPa)	dP_f/dt (MPa/min)	$d\sigma_n'/dt$ (MPa/min)	# Slip Events
Bc30	Berea	R	3.5×10^{-7}	61	−1	9.2	1.2	−3.3	2
B1	Berea	R	3.1×10^{-7}	58	−1	9.2	0.9	−3.1	3
B2	Berea	R	1.6×10^{-7}	58	−0.5	9.2	0.5	−1.6	3
B3	Berea	R	2.1×10^{-7}	55	−1	0, dry	0	−1.6	0
B4	Berea	R	2.1×10^{-7}	62	−1	9.2	0	−1.6	0
B5	Berea	R	1.6×10^{-7}	62	−0.5	9.2	0.5	−1.6	2
B6	Berea	C	1.8×10^{-7}	62	0	9.2	0.96	−1.5	0
Bc21	Berea	C	4.6×10^{-7}	52	0	9.2	0	0	0
Bc20	Berea	C	4.6×10^{-7}	42	0	0, dry	0	0	0
Bc25	Berea	C	4.6×10^{-7}	52	0	0, dry	0	0	0
DD1	Darley Dale	R	3.8×10^{-7}	58	−1	9.2	0.9	−3.0	2
DD2	Darley Dale	R	1.6×10^{-7}	58	−0.5	9.2	0.5	−1.6	4
DD3	Darley Dale	R	2.0×10^{-7}	58	−1	0, dry	0	−1.6	1
DD4	Darley Dale	R	2.0×10^{-7}	58	−1	9.2	0	−1.6	7
DD6	Darley Dale	C	6.5×10^{-7}	58	0	9.2	0.3	−0.5	0
DD7	Darley Dale	C	4.6×10^{-7}	58	0	9.2	0	0	0
DD8	Darley Dale	C	2.1×10^{-7}	62	0	9.2	0.9	−1.4	0

[a]R and C indicate lateral relaxation and axial compression tests, respectively. v is the imposed shear slip rate. σ_3 and P_f are the confining and pore pressures at the beginning of shearing.

2. Methods and Materials

We study slip along faults within two isotropic and homogeneous sandstones; the Berea sandstone and Darley Dale sandstone have high porosity and permeability that facilitate rapid diffusion of pore fluid through the samples (supporting information). The samples are sandstone cores 25.4 mm in diameter and 50.8 mm in length prepared with sawcut surfaces oriented $\theta = 30°$ to the axis of the cylindrical samples (Figure S1 in the supporting information).

The experiments were conducted in a triaxial deformation apparatus at room temperature. In this configuration the maximum principal stress (σ_1) is axial, and the minimum principal stress (σ_3) is radial. The pore fluid pressure is adjusted by a servocontrolled pressure intensifier connected at the upstream sample end. The spatial averages of the shear and effective normal stresses along the fault surface are determined from σ_1, σ_3, and P_f and are corrected for the reduction in elliptical area of the fault with increasing axial displacement [*Tembe et al.*, 2010, Appendix A]. The shear and effective normal stresses along the fault surface are

$$\tau = \frac{1}{2}(\sigma_1 - \sigma_3)\sin 2\theta \tag{1}$$

$$\sigma_n' = (\sigma_3 - P_f) + \frac{1}{2}(\sigma_1 - \sigma_3)(1 - \cos 2\theta) \tag{2}$$

We investigate fault slip under conditions of constant effective normal stress as well as decreasing effective normal stress, which was achieved either by changing the mechanical stresses (σ_1 and σ_3) or increasing the pore fluid pressure (P_f) during slip along the fault (equation (2)). During frictional sliding in the triaxial configuration, σ_3 is controlled and σ_1 is limited by the strength $\tau \leq \tau_C$. Loading rates are chosen to ensure that the rates of decreasing effective normal stress and shear stress and fault slip velocity are similar in all experiments (Table 1). Slip rates are corrected for elastic distortion of the apparatus (supporting information).

We employ the conventional "axial compression" path during which confining pressure is held constant while the axial piston advances to cause sliding along the saw cut surface. At constant pore fluid pressure, this stress path results in an increase in shear and normal stresses until stress reaches the frictional sliding envelope at which point sliding occurs at constant shear and normal stresses (Figures 1a, 2a, and 2b and Table 1).

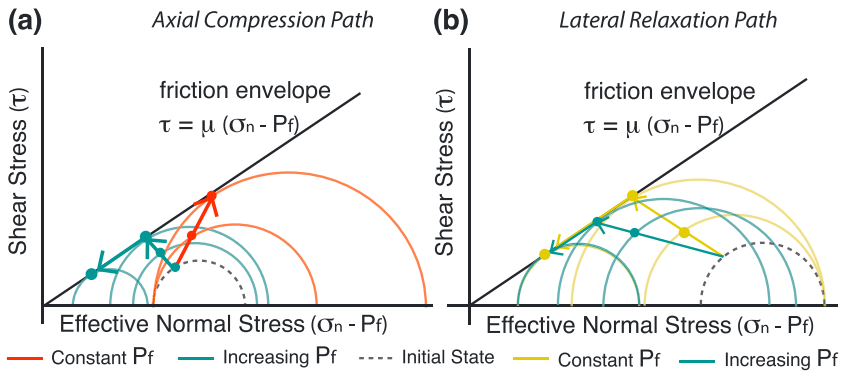

Figure 1. Mohr-Coulomb diagrams showing the evolution of stress with time along the simulated experimental faults. (a) Axial compression stress path with constant fluid pressure (orange) and increasing fluid pressure (green). (b) Lateral relaxation stress path with constant fluid pressure (yellow) and increasing fluid pressure (green).

Pore fluid pressure is increased during sliding along the fault in some axial compression experiments, which causes decreasing effective normal stress and shear stress owing to the reduction in τ_C according to $\frac{d\tau}{dt} = -\mu\frac{dP_f}{dt}$ (Figures 1a, 2c, and 2d and Table 1).

The second stress path we employ is the "lateral relaxation" path [e.g., *Tamarkin et al.*, 2012]. During this stress path, the sample is stressed until yield using the axial compression (i.e., until deviation of the stress-strain curve from linear indicating the onset of inelastic strain), which establishes an initial stress state within a typical seismic stress drop (a few MPa) of the friction envelope. The confining pressure is subsequently reduced at a constant rate as the axial piston is advanced. For both constant and increasing pore fluid pressure, the lateral relaxation path causes decreasing effective normal stress and increasing shear stress until frictional sliding occurs. During frictional sliding the effective normal stress decreases at the imposed rates and shear stress decreases according to $\frac{d\tau}{dt} = \mu\left(\frac{d\sigma_n}{dt} - \frac{dP_f}{dt}\right)$ (Figures 1b and 2e–2h). Mechanical loading is controlled so that the rate of shear stress decrease ($d\tau/dt$) in a lateral relaxation experiment is comparable to that in the corresponding axial compression experiment with increasing pore pressure.

We investigated frictional sliding under conditions of constant and decreasing effective normal stress using the axial compression and lateral relaxation paths (1) with constant pore fluid pressure, (2) with increasing pore fluid pressure at constant rate (0.5 MPa/min and 1.0 MPa/min), and (3) dry (Table 1).

3. Results

Fault slip occurs at a near-constant shear stress and normal stress during the axial compression tests conducted at constant pore fluid pressure (Figures 2a, 2b, and 3a). When pore fluids are injected at a constant rate, slip during axial compression occurs as effective normal stress and shear stress decrease (Figures 2c, 2d, and 3b). Fault slip during all axial compression tests is consistent with the threshold criterion and occurs at near-constant sliding velocity (Figures 3a, 3b, and S2).

The shear stress decreases during slip in all lateral relaxation tests as a result of the decreasing effective normal stress (Figures 2e–2h, 3c, and 3d). Episodes of accelerated fault slip occur during the lateral relaxation paths and do not occur during the axial compression paths (Figures 3d and S2). Slip events are evidenced by a decrease in shear stress that is more rapid than that caused by decreasing effective normal stress $\left(\text{i.e., } \frac{d\tau}{dt} = \mu\left(\frac{d\sigma_n}{dt} - \frac{dP_f}{dt}\right)\right)$. The shear stress drops range from 0.5 to 3.8 MPa (Figures 4a and S2). The Darley Dale sandstone experiences slip events under dry conditions as well as constant and increasing pore fluid pressure, and the Berea sandstone experiences slip events during pore fluid pressurization, but not dry or under constant pore fluid pressure.

When a slip event occurs during pore fluid pressurization, a rapid, uncontrolled, and permanent increase in the pore pressure is observed during the event (Figures 3d and S2); the increase in pore pressure is between 0.3 and 2.5 MPa and is on average 55% of the magnitude of the shear stress drop (Figure 4a). Only the tests with pore fluid injection exhibit a jump in pore fluid pressure during slip.

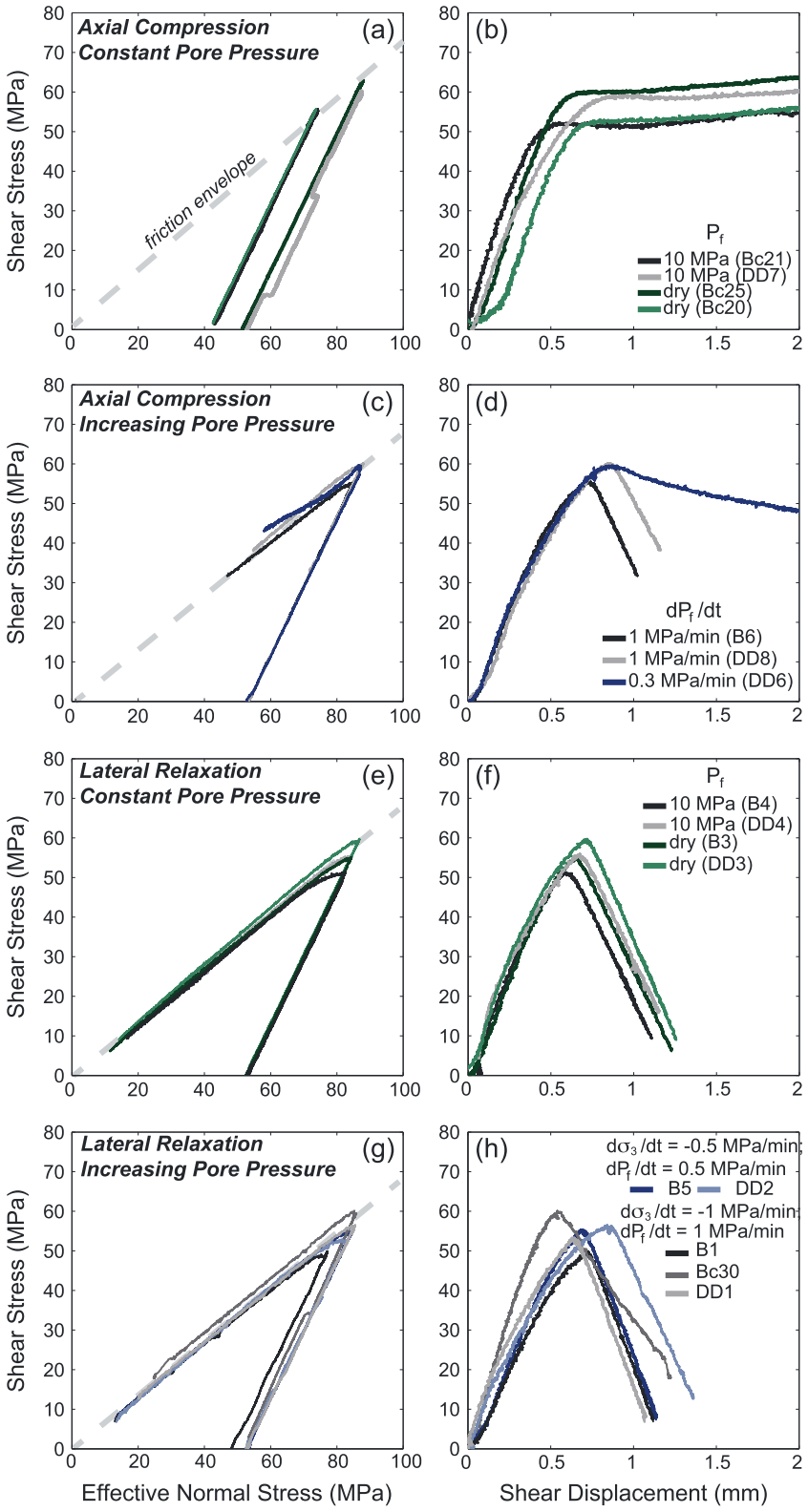

Figure 2. (a, c, e, and g) Shear stress and effective normal stress during sliding and (b, d, f, and h) shear stress evolution during sliding for (Figures 2a and 2b) axial compression stress path at constant fluid pressure, (Figures 2c and 2d) axial compression stress with increasing fluid pressure, (Figures 2e and 2f) lateral relaxation stress at constant fluid pressure, and (Figures 2g and 2h) lateral relaxation stress with increasing fluid pressure. Grey dashed lines indicate the friction envelope.

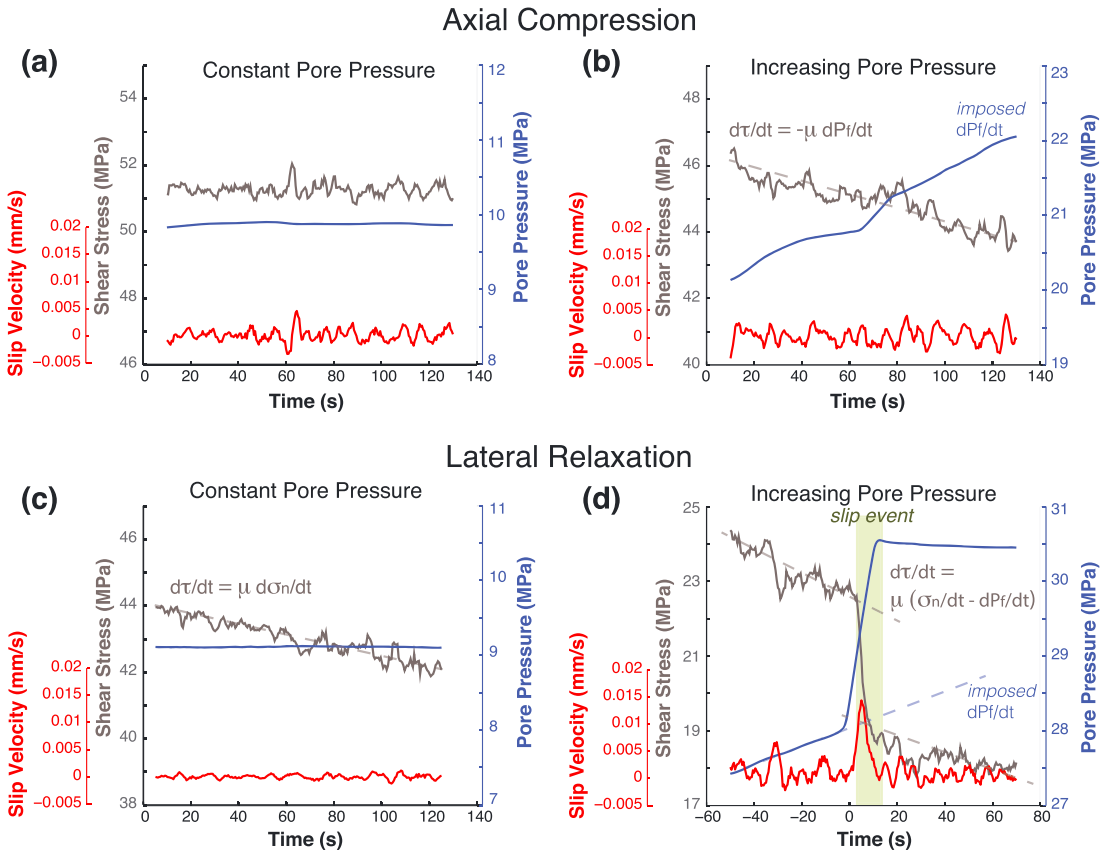

Figure 3. Examples of slip along faulted Berea sandstone under (a and b) axial compression and (c and d) lateral relaxation paths. Data are from four experiments shown in Figure 2. Shear stress (gray), pore pressure (blue), and slip velocity (red) are shown with time. Imposed slip velocity is $\sim 10^{-4}$ mm/s in all tests. (Figure 3a) Pore pressure is constant (9.2 MPa) (# Bc21; Table 1). (Figure 3b) Imposed pore pressurization at 1 MPa/min (# B6). (Figure 3c) Pore pressure is constant (9.2 MPa) (# B4). (Figure 3d) Pore pressurization rate is 1 MPa/min (dashed blue line). $t = 0$ s indicates the beginning of the slip event (shaded green) (# Bc30). All data are smoothed using a five-point moving average. Small-amplitude variations in shear stress and slip velocity are caused by electrical noise.

The highest rates of effective normal stress reduction during lateral relaxation correspond to the greatest slip, shear stress drop (uncontrolled), and slip rates (Figures 4a and 4b). Specifically, lateral relaxation tests conducted at the same rate of decrease in effective normal stress (~ -1.5 MPa/min) both entirely by mechanical changes in stress and by a combination of mechanical changes and an increase in pore fluid pressure exhibit similar slip behavior and shear stress changes (Figure 4a).

Fault slip rates increase up to 2 orders of magnitude during slip events and are generally highest during the highest rates of effective normal stress decrease (Figures 4b and S2). The magnitude of the fluid pressure increase is linearly correlated with slip rates (Figure 4b). The largest shear stress drops usually occur during the fastest reduction in effective normal stress, and the smallest stress drops occur under dry conditions. The magnitude of the stress drop is not correlated with the magnitude of the fluid pressure at the beginning of the event nor is it specific to either sandstone (Figure 4c).

In all of the experiments, shearing of the fault surfaces produces a granular gouge layer that is tenths of a millimeter thick. Although the fault surfaces have negligible cohesion at the beginning of an experiment, after shearing the fault surfaces and gouge are cohesive and must be pried apart. The gouge layers exhibit striations parallel to the slip direction (Figure S1d).

4. Discussion

4.1. Slip Acceleration Under Stress Paths of Decreasing Effective Normal Stress

The observation that with constant fluid pressure, slip events occur during the lateral relaxation paths and not the axial compression paths indicate decreasing normal stress and shear stress promote accelerated slip. This result can be explained by previous experimental observations and analyses which show that decreasing

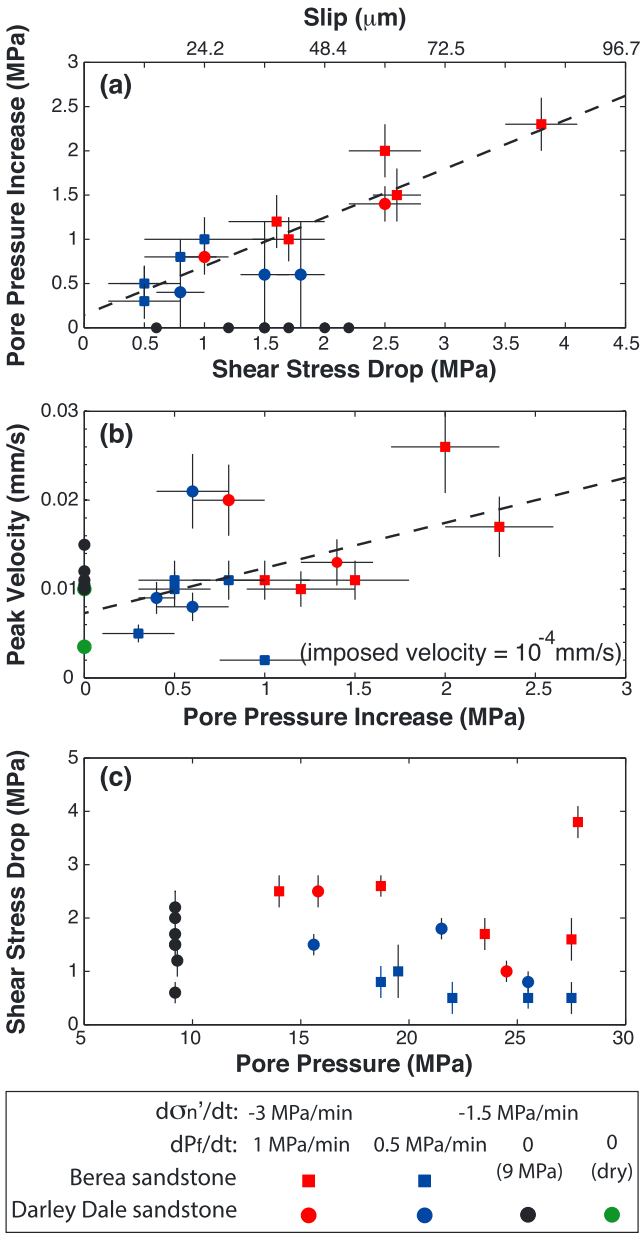

Figure 4. Correlations between slip event parameters and pore fluid pressure conditions during lateral relaxation tests. (a) The increase in pore pressure is defined as the magnitude of the pore pressure change during which the rate of change is greater than the imposed rate. The shear stress drop is defined as the magnitude of the shear stress change during which $-d\tau/dt > -\mu(d\sigma_n/dt - dP_f/dt)$. For fluid pressurization tests, a linear correlation exists between the pore pressure increase and shear stress drop (and slip). The rate of effective normal stress reduction roughly correlates with the magnitude of the shear stress drop. (b) Peak velocity is the maximum velocity calculated during a slip event (supporting information). Peak velocities are positively correlated with the pore pressure increase during an event (linear regression has a slope of 0.0051). Higher rates of effective normal stress reduction roughly correlate with higher peak slip velocities. (c) Shear stress drop is not correlated with the magnitude of the pore pressure at the beginning of the event. Error bars for pore pressure and shear stress changes were determined by visual inspection of the data and indicate the potential range of values caused by uncertainty in determining the initiation and end of a slip event. Error in velocity determination is the result of electrical noise and was determined as the standard deviation from a constant slip velocity calculated between slip events.

normal stress can cause unstable fault slip [*Linker and Dieterich*, 1992; *Dieterich and Linker*, 1992; *Chambon and Rudnicki*, 2001; *He and Wong*, 2014]. The instability is shown to occur because a decrease in the effective normal stress causes an immediate decrease in the friction coefficient and, therefore, shear stress ($\tau = \mu(\sigma_n - P_f)$) that is analogous to the direct effect in velocity-stepping tests followed by an increase in friction coefficient to steady state. Unstable slip caused by decreasing normal stress is, therefore, analogous to stick slip that occurs at constant normal stress in fault rocks with velocity-weakening frictional strength [*Gu et al.*, 1984]; for decreasing normal stress, however, unstable slip may occur along faults that exhibit velocity-strengthening friction [*Dieterich and Linker*, 1992]. Thus, the slip events that we report are most easily explained as being caused by decreasing normal stress associated with the lateral relaxation stress path.

Slip events that occur during the lateral relaxation tests have lower slip rates (< 0.1 mm/s) than those of typical stick-slip events observed during previously reported normal stress reduction tests or constant normal stress tests in velocity-weakening fault rock [*Johnson and Scholz*, 1976]. We infer that these events represent the nucleation of slow slip rather than seismogenic slip. This slow slip behavior may indicate that experimental conditions are near a transition between unstable and stable slip, as has been shown to exist under variable normal stress conditions much like geophysical observations of slow slip phenomena are proposed to occur near a transition from unstable to stable fault slip under velocity-weakening conditions [*He et al.*, 1998; *Perfettini et al.*, 2001].

The experimental results show that a reduction in mechanical stress is more efficient than increasing pore fluid pressure at initiating slip events even though both represent conditions of decreasing effective normal stress. This is consistent with experimental data of brittle faulting in intact rock samples [*Ougier-Simonin and Zhu*, 2015]. Specifically, despite the fact that the *effective* normal stress decreases at similar rates during axial compression stress paths with increasing pore fluid pressure and during all lateral relaxation stress paths, slip events only occur during lateral relaxation stress paths (Table 1). This result suggests fundamental differences in the effects of mechanical loading and pore fluid pressure on slip processes, contrary to the effective stress criterion for which the evolution of fluid pressure and normal stress are equivalent. We propose that whereas mechanical loading causes instantaneous and uniform changes in stress, changes in pore fluid pressure occur by diffusion which results in a gradual evolution of contact-scale stresses and spatially heterogeneous fluid pressure. Although the permeability of the sandstone is high (10^{-14} to 10^{-13} m^2), facilitating rapid diffusion of pore water to the fault zone, gouge layers produced by shearing of rock surfaces are shown to have permeability that is as low as 10^{-17} m^2 [*Zhang and Tullis*, 1998]. Thus, increasing pore fluid pressure may be less effective at inducing slip events because pore fluid pressure evolution has a more gradual and heterogeneous effect on the evolution of grain contact area and strength within the fault gouge.

4.2. Pore Pressure Evolution During Slip Acceleration

The increase in pore fluid pressure that occurs during slip events indicates that the sandstone rapidly compacts, and correlations between pore pressure increase and shear stress drop and peak velocity may indicate that this compaction-induced pressurization enhances slip (Figures 4a and 4b). Previous studies of faulted porous sandstone sheared under axial compression show a decrease in fluid pressure indicating dilation during the rapid slip portion of the stick-slip cycle, and the magnitude of depressurization is similar to that of the pressurization we observe in the lateral relaxation tests [*Logan*, 1978; *Teufel*, 1980]. On the other hand, stick-slip events in crystalline rocks and simulated fault gouges tested using the direct shear configuration occur synchronous with slight compaction during rapid sliding [*Sundaram et al.*, 1976; *Fulton and Rathbun*, 2011; *Scuderi et al.*, 2015]. When pore fluid pressure is monitored during direct shear tests, the magnitude of pressurization during compaction is 2 orders of magnitude smaller than that during the lateral relaxation tests in this study and is on the order of 10% of the magnitude of the shear stress drop, compared to 55% for slip events during lateral relaxation. The difference is likely caused in part by the decoupling of shear and normal stresses that are characteristic of the direct shear configuration or by the lower normal stresses often employed in the direct shear configuration. Nevertheless, comparison of porous rocks sheared in the triaxial configuration indicates that rapid slip during axial compression causes an increase in pore volume and depressurization of pore fluids, whereas slip in the lateral extension tests is accompanied by compaction and pressurization of the pore fluid.

Note that the stress states as well as the stress paths during the slip events are the same in the axial compression and lateral relaxation experiments; during slip events, the axial load (σ_1) decreases while confining

pressure (σ_3) remains approximately constant resulting in a decrease in both normal and shear stresses. Thus, differences in the pore volume changes that occur during slip events in the two experimental configurations must be caused by differences in porosity evolution that occur between slip events. It is inferred that between stick-slip events in conventional tests, the faulted rock undergoes elastic compaction, which is partially released and causes dilation and depressurization during the stick-slip event [*Logan*, 1978; *Teufel*, 1980]. By comparison, we infer that the faulted rock and gouge layer dilate between slip events in the lateral relaxation path, and compact as the strain is partially recovered during the slip event.

Higher imposed pressurization rates are inferred to enhance slip by increasing the rate of effective normal stress reduction. Evidence to support this inference is in the correlation between shear stress drop (and slip) and the rate of effective normal stress change (Figure 4a). Although slip events do not occur during axial compression even with fluid pressurization, the fluid pressurization during lateral relaxation does contribute to the size of these events; otherwise, the slip events in tests conducted at 1 MPa/min fluid injection and with constant fluid pressure would be expected to be similar in slip and slip velocity.

The lack of a correlation between shear stress drop and the magnitude of the pore fluid pressure (Figure 4c) indicates that the fluid pressure itself is not an important control on slip events. In contrast, there is a positive correlation between the shear stress drop and the imposed rate of effective normal stress reduction (Figure 4a), which indicates that fluid pressurization rate may be important in inducing slip events in that it enhances the rate of effective normal stress reduction.

4.3. Relevance to In Situ Stress Conditions

The results of this experimental study are consistent with previous studies which show that decreasing effective normal stress promotes accelerating slip, but modeling of fluid-induced seismicity using an effective stress criterion may overestimate the effectiveness of increased pore fluid pressure on triggering seismic slip. These results indicate that pore fluid pressurization is most likely to enhance slip rates under in situ boundary conditions of decreasing total normal stress. Fluid injection is shown to cause aseismic creep events that precede seismicity [*Guglielmi et al.*, 2015]. Under certain boundary conditions, such aseismic creep events may cause a decrease in fault normal stress that leads to seismicity during fluid injection, as demonstrated in these experiments. Changes in normal stress during slip may occur because of tectonic regime particularly where there are free boundary conditions, nonplanar fault geometry, and contrast in the elastic properties of wall rocks [*Chambon and Rudnicki*, 2001].

Studies of induced earthquakes are limited in their ability to constrain fluid pressure evolution in space and time, and it must, therefore, be inferred. As a result, estimates of the fluid pressure changes required to induce slip vary from less than 0.1 MPa to 10 MPa [*Terakawa et al.*, 2012; *Keranen et al.*, 2014]. Because fluid pressure cannot be monitored with sufficient spatial resolution, it is difficult to distinguish between the effects of fluid-injection rate and the absolute magnitude of pore fluid pressure, which is expected to correlate with and reflect injection rate. In our experiments, the pressurization rate is a critical control on slip behavior because it controls the rate of normal stress reduction independent of the fluid pressure magnitude, and this is consistent with known correlations between injection rates and the maximum size of triggered earthquakes [*Brodsky and Lajoie*, 2013; *Martinez-Garzon et al.*, 2014; *Frohlich et al.*, 2015]. *Bachmann et al.* [2012] correlate a higher frequency of smaller magnitude events with high injection rates, because it correlates with high pore fluid pressure. An alternative hypothesis is that the injection rate is itself the factor that enhances rates of microseismicity.

The heterogeneous permeability structure of fault zones is known to cause spatially variable fluid pressures over scales of meters to kilometers and to, therefore, control the spatial and temporal evolutions of fault slip during fluid diffusion [*Bachmann et al.*, 2012]. If fluids are less effective at inducing slip because fluid diffusion through fault gouge and surrounding rock is heterogeneous, as we hypothesize, then quantifying the pore structure and transient heterogeneous fluid pressure in the principal slip zone is as critically important to predicting induced seismicity as understanding regional permeability tensors. The multiscale nature of the problem is illustrated by observations that seismic slip occurs when fluid diffuses tens of kilometers through host rock into fault zones [*Keranen et al.*, 2014] as well as when fluid is pumped directly into the fault zone itself [*Horton*, 2012; *Kim*, 2013].

5. Conclusions

We investigated fault slip behavior under conditions of fluid pressurization. Although fault slip is well predicted to occur at a threshold shear stress that depends upon an effective normal stress, the style of slip is cannot be determined by a threshold criterion.

1. We show that decreasing effective normal stress induces accelerated slip events when accomplished by changes in mechanical stresses, but fluid pressurization alone is insufficient to induce slip events.
2. We propose that the differences reflect the fact that mechanical loading alters contact-scale stresses within the gouge layer in a manner that is both more rapid and uniform than occurs by changes in pore fluid pressure, which occurs by diffusion.
3. Compaction during slip enhances both the rate and magnitude of slip as a result of increasing the pore fluid pressure.
4. Pore fluid pressurization does enhance slip events induced by a mechanical reduction in normal stress. Under these conditions, the magnitude of slip, slip velocity, and shear stress drop all correlate with the rate of effective normal stress reduction. Thus, fluid pressurization is an important control on slip behavior in that it increases the rate of effective normal stress reduction.

Acknowledgments
This work is funded by DOE DE-FG02-07ER15916, NSF-EAR1056317 and NSF-EAR1452339. We benefited from discussions with V. Lekic and L. Montesi. We thank T. Tamarkin for technical support. Data are available from the corresponding author upon request.

References

Bachmann, C. E., S. Wiemer, B. P. Goertz-Allmann, and J. Woessner (2012), Influence of pore-pressure on the event-size distribution of induced earthquakes, *Geophys. Res. Lett.*, *39*, L09302, doi:10.1029/2012GL051480.

Brodsky, E., and L. Lajoie (2013), Anthropogenic seismicity rates and operational parameters at the Salton Sea geothermal field, *Science*, *341*(6145), 543–546, doi:10.1126/science.1239213.

Byerlee, J. (1978), Friction of rocks, *Pure Appl. Geophys.*, *116*(4–5), 615–26, doi:10.1007/BF00876528.

Chambon, G., and J. Rudnicki (2001), Effects of normal stress variations on frictional stability of a fluid-infiltrated fault, *J. Geophys. Res.*, *106*(B6), 11,353–11,372, doi:10.1029/2001JB900002.

Deichmann, N., and D. Giardini (2009), Earthquakes induced by the stimulation of an enhanced geothermal system below Basel, Switzerland, *Seismol. Res. Lett.*, *80*(5), 784–798, doi:10.1785/gssrl.80.5.784.

Dieterich, J., and M. Linker (1992), Fault stability under conditions of variable normal stress, *Geophys. Res. Lett.*, *19*(16), 1691–1694, doi:10.1029/92GL01821.

Ellsworth, W. (2013), Injection-induced earthquakes, *Science*, *341*(6142), 1225942, doi:10.1126/science.1225942.

Frohlich, C., J. I. Walter, and J. F. W. Gale (2015), Analysis of transportable array (USARRAY) data shows earthquakes are scarce near injection wells in the Williston Basin, 2008–2011, *Seismol. Res. Lett.*, *86*(2A), 492–499, doi:10.1785/0220140180.

Fulton, P. M., and A. P. Rathbun (2011), Experimental constraints on energy partitioning during stick-slip and stable sliding within analog fault gouge, *Earth Planet. Sci. Lett.*, *308*(1–2), 185–192, doi:10.1016/j.epsl.2011.05.051.

Gu, J.-C., J. Rice, A. Ruina, and S. Tse (1984), Slip motion and stability of a single degree of freedom elastic system with rate and state dependent friction, *J. Mech. Phys. Solids*, *32*(3), 167–96, doi:10.1016/0022-5096(84)90007-3.

Guglielmi, Y., F. Cappa, J.-P. Avouac, P. Henry, and D. Elsworth (2015), Seismicity triggered by fluid injection-induced aseismic slip, *Science*, *348*(6240), 1224–1226, doi:10.1126/science.aab0476.

He, C., and T.-f. Wong (2014), Effect of varying normal stress on stability and dynamic motion of a spring-slider system with rate- and state-dependent friction, *Earthquake Sci.*, *27*(6), 577–587, doi:10.1007/s11589-014-0098-4.

He, C., S. Ma, and J. Huang (1998), Transition between stable sliding and stick-slip due to variation in slip rate under variable normal stress condition, *Geophys. Res. Lett.*, *25*(17), 3235–3238, doi:10.1029/98GL02518.

Holland, A. A. (2013), Earthquakes triggered by hydraulic fracturing in south-central Oklahoma, *Bull. Seismol. Soc. Am.*, *103*(3), 1784–1792, doi:10.1785/0120120109.

Horton, S. (2012), Disposal of hydrofracking waste fluid by injection into subsurface aquifers triggers earthquake swarm in central Arkansas with potential for damaging earthquake, *Seismol. Res. Lett.*, *83*(2), 250–260, doi:10.1785/gssrl.83.2.250.

Hubbert, M. K., and W. W. Rubey (1959), Mechanics of fluid-filled porous solids and its application to overthrust faulting, [part] 1 of role of fluid pressure in mechanics of overthrust faulting, *Geol. Soc. Am. Bull.*, *70*(2), 115–166, doi:10.1130/0016-7606(1959)70[115:ROFPIM]2.0.CO;2.

Johnson, T. L., and C. H. Scholz (1976), Dynamic properties of stick-slip friction of rock, *J. Geophys. Res.*, *81*(5), 881–888, doi:10.1029/JB081i005p00881.

Keranen, K. M., H. M. Savage, G. A. Abers, and E. S. Cochran (2013), Potentially induced earthquakes in Oklahoma, USA; Links between wastewater injection and the 2011 M_W 5.7 earthquake sequence, *Geology*, *41*(6), 699–702, doi:10.1130/G34045.1.

Keranen, K. M., M. Weingarten, G. A. Abers, B. A. Bekins, and S. Ge (2014), Sharp increase in central Oklahoma seismicity since 2008 induced by massive wastewater injection, *Science*, *345*(6195), 448–451, doi:10.1126/science.1255802.

Kim, W.-Y. (2013), Induced seismicity associated with fluid injection into a deep well in Youngstown, Ohio, *J. Geophys. Res. Solid Earth*, *118*, 3506–3518, doi:10.1002/jgrb.50247.

Linker, M. F., and J. H. Dieterich (1992), Effects of variable normal stress on rock friction: Observations and constitutive equations, *J. Geophys. Res.*, *97*(B4), 4923–4940, doi:10.1029/92JB00017.

Logan, J. (1978), Creep, stable sliding, and premonitory slip, *Pure Appl. Geophys.*, *116*(4-5), 773–789, doi:10.1007/BF00876538.

Majer, E. L., R. Baria, M. Stark, S. Oates, J. J. Bommer, B. Smith, and H. Asanuma (2007), Induced seismicity associated with enhanced geothermal systems, *Geothermics*, *36*(3), 185–222, doi:10.1016/j.geothermics.2007.03.003.

Martinez-Garzon, P., G. Kwiatek, H. Sone, M. Bohnhoff, G. Dresen, and C. Hartline (2014), Spatiotemporal changes, faulting regimes, and source parameters of induced seismicity: A case study from the Geysers geothermal field, *J. Geophys. Res. Solid Earth*, *119*, 8378–8396, doi:10.1002/2014JB011385.

McGarr, A. (1976), Seismic moments and volume changes, *J. Geophys. Res.*, *81*(8), 1487–1494, doi:10.1029/JB081i008p01487.

McGarr, A. (2014), Maximum magnitude earthquakes induced by fluid injection, *J. Geophys. Res. Solid Earth*, *119*, 1008–1019, doi:10.1002/2013JB010597.

Ougier-Simonin, A., and W. Zhu (2015), Effect of pore pressure buildup on slowness of rupture propagation, *J. Geophys. Res. Solid Earth*, *120*, 7966–7985, doi:10.1002/2015JB012047.

Perfettini, H., J. Schmittbuhl, J. R. Rice, and M. Cocco (2001), Frictional response induced by time-dependent fluctuations of the normal loading, *J. Geophys. Res.*, *106*(B7), 13,455–13,472, doi:10.1029/2000JB900366.

Petersen, M., et al. (2015), Incorporating induced seismicity in the 2014 United States national seismic hazard model-results of 2014 workshop and sensitivity studies: U.S. Geological Survey open-file report 2015–1070, *Tech. Rep.*, U.S. Geol. Surv., doi:10.3133/ofr20151070.

Scuderi, M. M., B. M. Carpenter, P. A. Johnson, and C. Marone (2015), Poromechanics of stick-slip frictional sliding and strength recovery on tectonic faults, *J. Geophys. Res. Solid Earth*, *120*, 6895–6912, doi:10.1002/2015JB011983.

Sundaram, P. N., R. E. Goodman, and C.-Y. Wang (1976), Precursory and coseismic water-pressure variations in stick-slip experiments, *Geology*, *4*, 108, doi:10.1130/0091-7613(1976)4<108:PACWVI>2.0.CO;2.

Tamarkin, T., A. Ougier-Simonin, and W. Zhu (2012), Progressive microscopic damage associated with fault growth, *Geophys. Res. Lett.*, *39*, L15303, doi:10.1029/2012GL052487.

Tembe, S., D. A. Lockner, and T.-F. Wong (2010), Effect of clay content and mineralogy on frictional sliding behavior of simulated gouges: Binary and ternary mixtures of quartz, illite, and montmorillonite, *J. Geophys. Res.*, *115*, B03416, doi:10.1029/2009JB006383.

Terakawa, T., S. A. Miller, and N. Deichmann (2012), High fluid pressure and triggered earthquakes in the enhanced geothermal system in Basel, Switzerland, *J. Geophys. Res.*, *117*, B07305, doi:10.1029/2011JB008980.

Teufel, L. W. (1980), Precursive pore pressure changes associated with premonitory slip during stick-slip sliding, *Tectonophysics*, *69*(1–2), 189–199.

Weingarten, M., S. Ge, J. W. Godt, B. A. Bekins, and J. L. Rubinstein (2015), High-rate injection is associated with the increase in U.S. mid-continent seismicity, *Science*, *348*(6241), 1336–1340, doi:10.1126/science.aab1345.

Zhang, S., and T. E. Tullis (1998), The effect of fault slip on permeability and permeability anisotropy in quartz gouge, *Tectonophysics*, *295*(1–2), 41–52, doi:10.1016/S0040-1951(98)00114-0.